A Quasiclassical Trajectory Study of the Cl + HCN → HCl + CN Reaction Dynamics. Microscopic Reaction Mechanism of the H(Cl) + HCN → H_2(HCl) + CN Reactions†

Diego Troya

Departamento de Química, Universidad de La Rioja, C/Madre de Dios 51, 26006 Logroño, Spain

Miguel González*

Departamento de Química Física i Centre de Recerca en Química Teòrica, Universitat de Barcelona, C/Martí i Franquès 1, 08028 Barcelona, Spain

Guosheng Wu and George C. Schatz*

Department of Chemistry, Northwestern University, 2145 Sheridan Road, Evanston, Illinois 60208-3113

Received: September 18, 2000; In Final Form: November 8, 2000

The Cl + HCN → HCl + CN reaction dynamics has been studied using the quasiclassical trajectory method. The potential energy surface is taken from an accurate global surface for the HHCN system. Cl + HCN and H + HCN have very similar energetics, so the present calculation provides a test of whether the Cl + HCN dynamics is captured by a model in which the only difference is provided by the mass of the attacking atom. We find generally good agreement with experimental studies of the Cl + HCN reaction, including CN product rovibrational distributions and the relative rate coefficients for HCN initially in highly excited vibrational states. The results correctly describe the differences between Cl and H attack, so apparently the differences in the reactivity of these two reactions are a kinematic effect. A detailed analysis of the microscopic reaction mechanism of the H + HCN → H_2 + CN and Cl + HCN → HCl + CN reactions is also provided. This shows that the H and Cl reactions are both dominated by direct dynamics; however, the direct reaction with Cl frequently involves secondary collisions in which the Cl interacts with the CN fragment of HCN before abstracting the H atom, while the H atom reaction rarely does this. This allows the CN stretch mode to interact more strongly with reaction coordinate motions in Cl + HCN than in H + HCN, leading to greater CN vibrational excitation for initial HCN states that have no C−N stretch excitation, in agreement with observations.

I. Introduction

The lack of analytic potential energy surfaces (PESs) for polyatomic systems is a serious problem for reaction dynamics studies, even for tetratomic systems. There are several accurate analytic PESs for three-atom systems, and the methodologies for obtaining them can be regarded as well established. An often used method for obtaining three-atom analytical PESs is the fitting of ab initio data to flexible multiparametric functions.[1] This approach can be used for four atoms or more, but in reality very few reliable four-atom analytical PESs have been developed by this or any other method. One of the few available is that for the HHCN system.[2] In a recent paper,[3] the quasiclassical trajectory (QCT) method has been employed to study reaction dynamics in the atom + triatom system H + HCN → H_2 + CN on this surface (denoted the TSH3 PES hereafter). The accuracy of this surface had previously been demonstrated using different dynamics procedures, such as QCT calculations[2,4,5] and time-independent[6,7] and time-dependent[8,9] quantum dynamics (QM) calculations for the H_2 + CN → H + HCN reaction. For H + HCN, similar quality results were found, including good comparisons of CN internal distributions when compared with the experimental data. As a further extension of studies of the H + HCN → H_2 + CN reaction dynamics, in this paper we consider the adequacy of the TSH3 PES to describe the reaction dynamics of the analogous Cl + HCN → HCl + CN system.

While it is a bit unusual to simply substitute the potential energy surface of one reaction for another, there are some important similarities between these two surfaces that make this a sensible model in this case. Both surfaces have similar topologies,[10] including the same stationary points. These stationary point energies are compared in Figure 1. We see that the H + HCN → H_2 + CN and Cl + HCN → HCl + CN reactions have very similar endoergicities (22.4 ± 0.4 and 22.6 ± 0.4 kcal mol^{-1}, respectively[11]). The TSH3 analytical PES has an endoergicity of 21.3 kcal mol^{-1}, which is close to the values of both reactions. The activation energy of the Cl + HCN reaction may be inferred from experimental rate constant measurements on the reverse reaction,[12,13] along with the endoergicity just given, resulting in the value 27 kcal mol^{-1}. This value is reasonably close to the zero-point-corrected barrier for H + HCN, which is 23.9 kcal mol^{-1} on the TSH3 PES. There are also similarities concerning the XHCN (X = H, Cl) minimum (of C_{2v} symmetry in the X = H case), which is energetically below the X + HCN reagents for both reactions. The barrier on the TSH3 PES associated with the reaction path which leads from the atom + triatom asymptote to that minimum is 3.7 kcal

† Part of the special issue "Aron Kuppermann Festschrift".

* To whom correspondence should be addressed. E-mail: (M.G.) miguel@qf.ub.es, (G.C.S.) schatz@chem.nwu.edu.

10.1021/jp003371a CCC: $20.00
Published on Web 01/30/2001

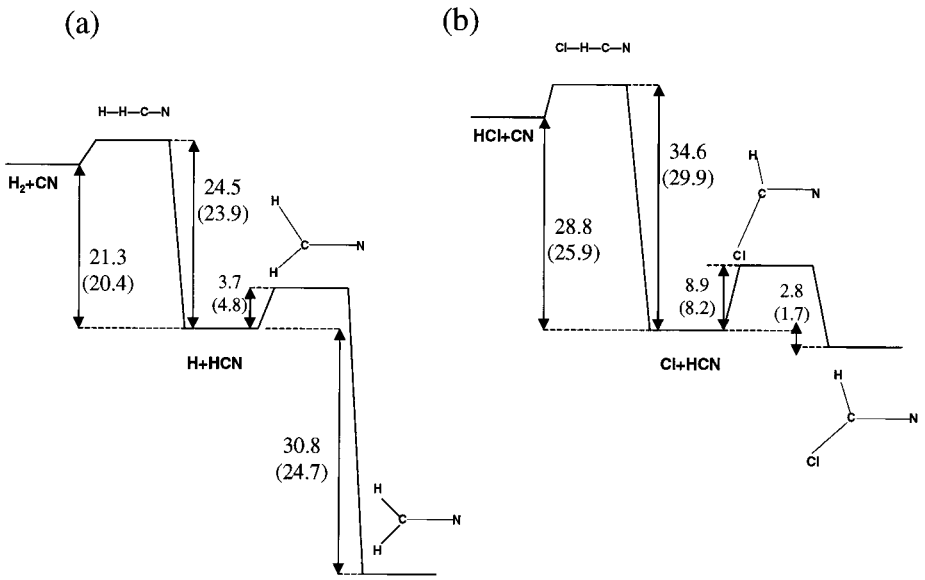

Figure 1. Schematic energy level diagram, showing the important stationary points for the H + HCN (a) and Cl + HCN (b) reactions. The H + HCN energies (kcal mol^{-1}) (zero-point-corrected results in parentheses) are taken from the TSH3 surface, while those for Cl + HCN are from the ab initio calculations of ref 10.

mol^{-1}. The corresponding ab initio value for the Cl + HCN reaction is 8.9 kcal mol^{-1}.[10] The depths of the well are nevertheless different for the two reactions. The TSH3 PES minimum is placed 30.8 kcal mol^{-1} below the reactants, according to ab initio results for the HHCN system, whereas the ClHCN minimum is only 3.5 kcal mol^{-1} more stable than the reactants.[10] However, earlier studies of the H + HCN → H_2 + CN reaction mechanism prove that the reaction pathway involving the HHCN minimum is unimportant at the energies relevant to the experiments, and the corresponding product state distributions are not affected by the reactivity through this minimum.[3] Thus, it is expected that the ClHCN minimum will not play a key role in the final state distributions of the HCl + CN products. The extensive ab initio study carried out by Harding on the ClHCN system[10] also considered the possibility of forming the ClHCN minimum through reaction pathways involving *cis*- and *trans*-ClCNH minima, as previously calculated in ref 14. These minima are also considered in the TSH3 surface for the HHCN system, and we have found in recent QCT studies[3] that the contribution of these pathways to the H_2 + CN reactivity is negligible at the energies considered in this study. These results suggest that it may be realistic to model Cl + HCN using the H + HCN potential surface and a mass of 35 amu for the attacking atom.

Additional reasons that encourage this study include the rich experimental information available for the Cl + HCN reaction. In many experimental references which deal with the study of the H + HCN → H_2 + CN reaction, the Cl + HCN → HCl + CN reaction has also been considered. For example, CN rovibrational distributions have been measured for the title reaction for several initial HCN states and translational energies,[15−18] as have been relative HCN vibrational state selected rate constants.[17,18] Furthermore, the experimental studies of the microscopic reaction mechanisms from the analysis of the CN product state distributions have raised important questions concerning whether the CN is a spectator or not, and concerning the relative importance of direct and addition−elimination mechanisms in both the H and Cl reactions with vibrationally excited HCN. Preliminary results of Gericke and co-workers[17] suggested that the CN fragment was active in the Cl + HCN → HCl + CN collision process. These results were subsequently superseded by more complete recent work of the same group.[18] The final conclusions from a larger number of initial HCN states led to a qualitative spectator model for the nonreacting CN bond. However, this conclusion is at odds with the Crim group results,[16] which suggested that the CN fragment is much less of a spectator for the Cl reaction than for the H reaction. In that experimental work, the CN nonspectator behavior was assumed to be due to the influence of the addition−eliminatiom mechanism (involving ClHCN formation as an intermediate complex). The present QCT study of the reaction mechanism using the model PES proposed here will elucidate the extent to which the spectator model applies to the CN fragment involved in these reactions.

The rest of the paper is organized as follows. Section II gives computational details. Section III compares the QCT results for the Cl + HCN → HCl + CN reaction with experimental results. Section IV compares Cl and H results in the reactions with HCN. Section V presents a detailed study of the microscopic reaction mechanism. The conclusions are summarized in section VI.

II. Computational Details

The parameters of the trajectory calculations were taken to be the same as those in the previous H + HCN QCT study.[3] The initial distance of the Cl atom to the HCN center of mass was fixed at 10 a_0. The interaction energy at this distance in the most repulsive geometrical arrangement of reactants (collinear Cl−N−C−H geometry) is 0.6 kcal mol^{-1}. This energy is below the 2% of the total initial energy considered in most of the calculations. The integration step used, 5 (time) atomic units (1.2×10^{-16} s), allows for total energy and total angular momentum conservation throughout the trajectories within at least four figures. Using the same initial distance between reactants and the same integration step as used in the H + HCN QCT calculation makes the Cl + HCN integration 6 times slower due to the mass change. The average number of integration time steps for the most common translational energy used (0.259 eV) is around 6000. In all, we have integrated over 750 000 trajectories to take into account all the HCN vibrational states for which there is experimental information available.

The maximum impact parameters were chosen to be at least 0.5 a_0 longer than the maximum reactive impact parameter

TABLE 1: CN Vibrational Populations for the Cl + HCN(v_1,0,v_3,j=9) → HCl + CN(v') Reaction under Different Initial Conditions[a]

HCN state	E_T		$v'=0$	$v'=1$	$v'=2$	$v'=3$	$\langle E_{VIB}\rangle$[b]
002	8.6	exptl[17,18]	0.86	0.13	<0.01		0.88
002	8.6	QCT	0.87 ± 0.12	0.13 ± 0.04			0.76 ± 0.15
004	8.6	exptl[17]	0.51	0.34	0.15		3.73
004	8.6	QCT	0.54 ± 0.04	0.30 ± 0.03	0.14 ± 0.02	0.02 ± 0.01	3.74 ± 0.55
004	6.0	exptl[17,18]	0.52	0.34	0.14	<0.02	3.66
004	6.0	exptl[16]	0.56	0.33	0.11		3.24
004	6.0	QCT	0.58 ± 0.05	0.31 ± 0.03	0.09 ± 0.02	0.02 ± 0.01	3.21 ± 0.46
302	6.0	exptl[17,18]	0.45	0.43	0.12	<0.02	3.90
302	6.0	exptl[16]	0.47	0.41	0.12		3.86
302	6.0	QCT	0.53 ± 0.06	0.32 ± 0.05	0.12 ± 0.03	0.03 ± 0.01	3.80 ± 0.61
402	6.0	exptl[18]	0.68	0.25	0.07	<0.02	2.32
402	6.0	QCT[c]	0.30 ± 0.03	0.35 ± 0.04	0.22 ± 0.03	0.08 ± 0.02	6.01 ± 0.81
104	6.0	exptl[18]	0.71	0.23	0.06	<0.02	2.01
104	6.0	QCT	0.58 ± 0.05	0.28 ± 0.03	0.11 ± 0.02	0.03 ± 0.01	3.44 ± 0.40
005	6.0	exptl[18]	0.41	0.38	0.15	0.06	5.11
005	6.0	QCT	0.42 ± 0.04	0.32 ± 0.03	0.20 ± 0.02	0.06 ± 0.02	5.26 ± 0.55
105	6.0	exptl[17,18]	0.65	0.25	0.10	<0.02	2.63
105	6.0	QCT	0.56 ± 0.03	0.22 ± 0.02	0.12 ± 0.01	0.10 ± 0.01	4.38 ± 0.48
006	6.0	exptl[18]	0.34	0.34	0.23	0.09	6.21
006	6.0	QCT[d]	0.45 ± 0.03	0.21 ± 0.02	0.13 ± 0.01	0.12 ± 0.01	6.94 ± 0.90

[a] All the energies are in kcal mol^{-1}. The uncertainties in the experimental vibrational populations are about ±0.03 for refs 17 and 18 and ±4% for ref 16. The experimental and QCT E_T values correspond to the average of the experimental collisional energies distribution. [b] The $\langle E_{VIB}\rangle$ values correspond to zero-point-subtracted average vibrational energies (see ref 3). Some initial zero-point-subtracted HCN internal energies are (kcal mol^{-1}) HCN(002) = 18.9, HCN(004), HCN(302) = 36.3, and HCN(402), HCN(104) = 42.3. [c] The CN QCT vibrational population in CN(v'=4), 0.05 ± 0.01, has been included in the average vibrational energy computation. [d] The CN QCT vibrational population in CN(v'=4), 0.09 ± 0.01, has been included in the average vibrational energy computation.

(b_{max}). We have used a uniform sampling between 0 and b_{max} instead of the customary uniform sampling between 0 and b^2_{max}. This reduces significantly the number of trajectories calculated in the nonreactive region of the opacity function, thus decreasing the computing effort. The proper calculation of the dynamics properties has been achieved by weighting each reactive trajectory by a factor associated with its initial impact parameter.

The comparison with experiment has required calculations with HCN in several rovibrational states. The rotational state throughout the work was taken to be j(HCN) = 9, to be consistent with the measurements of Gericke and co-workers.[17,18] The initial conditions of the HCN have been selected using vibrational and rotational action calculations explained elsewhere.[19,20] The high excitation considered in the HCN molecule (up to HCN(006)) requires following the time dependence of the actions until an accuracy of ±0.025$\hbar$ is achieved. This level of convergence has been considered in other recent work by several of us.[21]

In the calculation of the average rovibrational energy of the CN product, we have used the same procedure explained in the H + HCN work,[3] to make contact with the experiments. Here the product zero-point energy was not constrained in the calculations. The rovibrational populations of the CN product are almost invariant to zero-point energy restrictions on the partner diatom product. Therefore, we have not applied any restriction based on the HCl energy.

III. Comparison with Experimental Results

The best way to validate the assumptions made in this work is to compare the QCT results for Cl + HCN obtained using the TSH3 potential with the available experimental data. The wealth of results from Crim and co-workers[15,16] and Gericke and co-workers[17,18] concerning the CN rovibrational populations generated in the Cl + HCN → HCl + CN reaction allows for an extensive comparison with the QCT data. Up to eight initial HCN vibrational states have been experimentally explored, including highly excited ones. Table 1 presents the experimental and QCT CN vibrational distributions arising from the title reaction with these different initial conditions.

The agreement between the experimental and QCT CN vibrational distributions shown in Table 1 is generally good, with the differences between both sets of results often within the QCT uncertainties. Note in particular the excellent agreement for pure C−H stretch excited states of HCN, and also that for HCN(004) the change in the results on going from 6.0 to 8.6 kcal mol^{-1} translational energy matches experiment quite accurately. In fact, the only serious discrepancy between theory and experiment is for the HCN(402) state, where the QCT method predicts a CN vibrational distribution more excited than the one observed experimentally.[18] Indeed, the QCT prediction for this state indicates higher CN excitation than for HCN(302), while the experiment shows (surprisingly) just the opposite. The HCN(105) and HCN(104) results also present poorer agreement with experiment. The TSH3 analytical PES is therefore not able to reproduce results for high CN stretch excitations.

The results in Table 1 also provide some information on whether CN is a spectator or not. In particular, we notice that there is at least moderate vibrational excitation of the CN product for reagents with modest translational energy and no initial excitation of the C−N mode of the HCN reagent. For the HCN(004) reaction, around 30% of the CN population is formed in the CN(v'=1) state. This suggests that the C−N mode is somehow coupled to the reaction coordinate. We defer a study of this point until section IV.

To further test the adequacy of the PES used here to describe CN generation in the reaction of vibrationally excited HCN with chlorine, the CN diatomic product rotational distributions have also been compared with the available experimental data (Table 2). The experimental distributions can be well characterized by a single rotational temperature using fits to Maxwell−Boltzmann distributions. However, in the case of the QCT distributions,

TABLE 2: CN Average Rotational Energies for the Cl + HCN(v_1,0,v_3,j=9) → HCl + CN(v',j') Reaction under Different Initial Conditions[a]

HCN state	E_T		$\sum v'$	$v'=0$	$v'=1$	$v'=2$	$v'=3$
002	8.6	exptl[17]	3.14 ± 0.08	3.37 ± 0.08	1.86 ± 0.10		
002	8.6	QCT	0.51 ± 0.11	0.53 ± 0.13	0.39 ± 0.16		
004	8.6	exptl[17]	1.72 ± 0.10	1.80 ± 0.10	1.66 ± 0.08	1.47 ± 0.07	
004	8.6	QCT	1.35 ± 0.25	1.45 ± 0.37	1.35 ± 0.45	1.05 ± 0.35	0.90 ± 0.35
004	6.0	exptl[17]	1.70 ± 0.12	1.78 ± 0.12	1.62 ± 0.10	1.62 ± 0.32	
004	6.0	exptl[16]	1.60 ± 0.30				
004	6.0	QCT	1.21 ± 0.23	1.34 ± 0.30	1.03 ± 0.34	1.12 ± 0.42	0.47 ± 0.25
302	6.0	exptl[17]	1.53 ± 0.12	1.62 ± 0.12	1.50 ± 0.10	1.31 ± 0.25	
302	6.0	exptl[16]	2.00 ± 0.30				
302	6.0	QCT	1.05 ± 0.25	1.27 ± 0.40	0.85 ± 0.28	0.67 ± 0.26	1.01 ± 0.54
402	6.0	exptl[18]	1.43 ± 0.10	1.44 ± 0.10	1.41 ± 0.10	1.39 ± 0.10	
402	6.0	QCT	1.40 ± 0.30	2.25 ± 0.80	1.01 ± 0.28	1.11 ± 0.35	0.80 ± 0.27
104	6.0	exptl[18]	1.43 ± 0.10	1.44 ± 0.10	1.41 ± 0.10	1.39 ± 0.10	
104	6.0	QCT	1.42 ± 0.23	1.44 ± 0.31	1.51 ± 0.39	1.22 ± 0.44	1.43 ± 0.60
005	6.0	exptl[18]	1.42 ± 0.10	1.41 ± 0.10	1.48 ± 0.10	1.43 ± 0.10	1.05 ± 0.11
005	6.0	QCT	1.67 ± 0.32	1.74 ± 0.50	1.70 ± 0.51	1.57 ± 0.53	1.44 ± 0.63
105	6.0	exptl[17]	1.43 ± 0.10	1.44 ± 0.05	1.39 ± 0.13	1.27 ± 0.12	
105	6.0	QCT	1.71 ± 0.25	1.66 ± 0.32	1.84 ± 0.50	1.94 ± 0.65	1.67 ± 0.59
006	6.0	exptl[18]	1.34 ± 0.07	1.47 ± 0.05	1.21 ± 0.05	1.37 ± 0.12	1.31 ± 0.12
006	6.0	QCT	1.90 ± 0.36	1.67 ± 0.42	2.34 ± 0.78	2.39 ± 0.87	1.87 ± 0.68

[a] All the energies are in kcal mol^{-1}. The experimental and QCT E_T values correspond to the average of the experimental collisional energies distribution.

the large statistical uncertainties associated with the highly excited rotational levels of CN make the fitting process impractical. Hence, the information about rotation which can better be compared between theory and experiment is the average rotational energy.

Although CN rotation is in principle a more demanding requirement for the analytical PES, the reasonable agreement between experiment and most of the QCT results shown in Table 2 supports the plausibility of the TSH3 PES for treating the Cl + HCN → HCl + CN reaction. Included in the table are comparisons both for individual CN vibrational states and for the average over all the vibrational states. For most of the comparisons provided, the results for both quantities match within 40%. However, the comparison for HCN(002) is poor. Whereas it was experimentally observed[17,18] that for HCN(002) the CN is more rotationally excited than for the rest of the HCN levels studied, the QCT data are similar to what we find for the other HCN states. The Cl + HCN(006) product CN QCT rotation is also more excited than seen in the experimental measurements.[18] This is part of a trend in which the QCT calculations predict increasing CN rotational excitation with increasing C−H stretch excitation (comparing (004), (005), and (006) at 6 kcal mol^{-1}), while experiment shows the opposite result.

Some insights into the behavior of CN rotation can also be achieved by considering the correlation between reagent HCN rotational excitation and product CN excitation. The results in Table 2 indicate that the CN product is significantly more rotationally excited than thermal (300 K) CN ($\langle E_{ROT}\rangle = k_B T =$ 0.60 kcal mol^{-1}). This suggests that CN product rotational excitation arises from energy released during reaction rather than from the reagent HCN. This is in contrast to what we found in studies of the H + HCN → H_2 + CN reaction,[3] where the initial rotational excitation of HCN strongly influences the product CN rotational distribution. We will discuss this comparison with H + HCN further in the next section as it reveals important features about the differences between the two reactions. In the present Cl + HCN QCT calculations, the reagent HCN has a fixed-value initial rotational quantum number, j(HCN) = 9, that matches the value used in the experiments.[17,18] This value is a bit colder than the average thermal (300 K) j(HCN) value (12), so the HCN initial rotation has an even smaller effect on the CN product rotation in these experiments than might be expected.

The experimental results concerning the Cl + HCN reaction also include several relative rate constants associated with different HCN initial states.[17,18] This is in contrast to the H + HCN reaction, where such information is not available. We have calculated the rate constants for different initial HCN states from the excitation functions (cross sections vs relative translational energy), which are presented in Figure 2 for the HCN initial states investigated in this work. These excitation functions have the usual shape for a reaction with threshold energy,[22] with an approximate linear increase in the cross sections with energy above the threshold and then a bending over at higher energy. With one exception, a decrease in threshold energy on going from one state to another is correlated with an increase in the plateau value of the cross section. The exception to this behavior arises for HCN(302), which has a lower threshold and a lower plateau than HCN(402).

Table 3 presents the QCT relative rate constants that were derived from the excitation functions, along with experimental[17,18] results for Cl + HCN(v_1,0,v_3,j=9) → HCl + CN. The error bars in the QCT results are based on statistical uncertainties in the cross sections. Due to the assumptions made in this work and the possible zero-point energy leakage involved in the QCT calculations, highly accurate rate constants are not expected to be obtained, and the error bars do not indicate the absolute accuracy of the rate constants. Nevertheless, the major interest of the rate constant calculation lies in the relative values for different HCN states, and these should be realistic.

This table shows that the agreement of the results with experiment for the ratios of HCN(004) to HCN(302) and HCN(104) is quite good. Note that the k_{004}/k_{104} value is greater than unity in both the experiment and the QCT results (admittedly with large error bars in the latter). Apparently, adding a quantum of CN vibrational excitation to the HCN(004) state impedes reactivity rather than promotes it. The displacement of the threshold energies for these two states can be clearly seen in the inset of Figure 2.

One aspect of the QCT results in Table 3 that does not agree

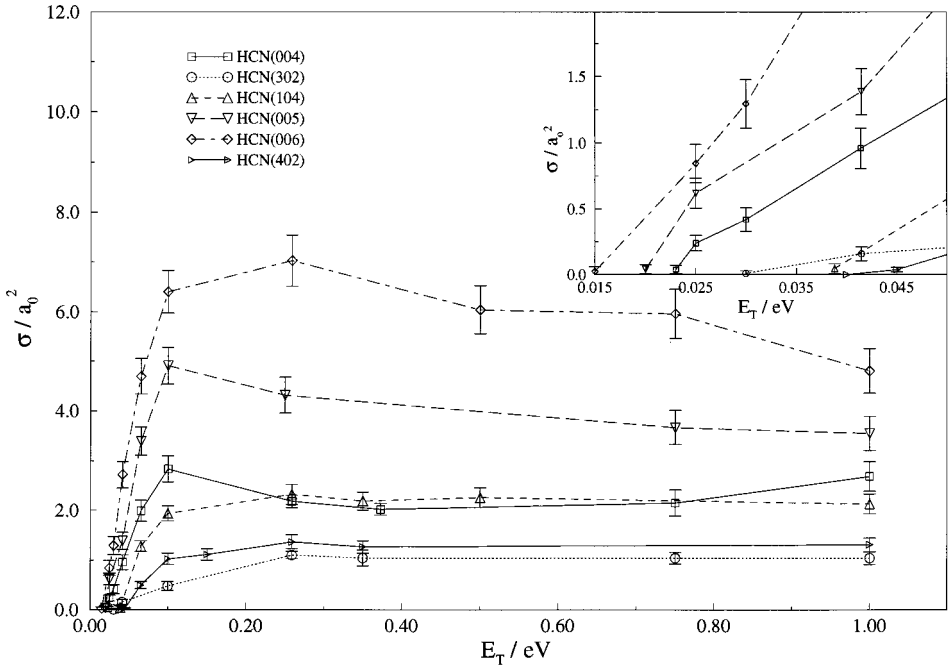

Figure 2. Excitation function (cross section vs translational energy) for the Cl + HCN(v_1,0,v_3,j=9) → HCl + CN reaction. The inset shows a blowup of the threshold region.

TABLE 3: Experimental and QCT Thermal (300 K) Relative Rate Constants for Cl + HCN(v_1,0,v_3,j=9) → HCl + CN with Different Initial HCN Vibrational States

	exptl	QCT		exptl	QCT
k_{004}/k_{104}	1.25 ± 0.4[18]	1.1 ± 0.2	k_{006}/k_{004}	7.9 ± 0.5[a]	2.8 ± 0.4
k_{004}/k_{302}	2.8 ± 0.6[17]	3.0 ± 0.3	k_{302}/k_{402}	0.45 ± 0.25[a]	2.2 ± 0.5
k_{005}/k_{004}	4.1 ± 0.5[a]	1.7 ± 0.3			

[a] Experimental ratios estimated from Table 3 and Figure 2 of ref 18.

quantitatively with experiment is the ratios associated with HCN(005) and HCN(006) relative to HCN(004). The table shows that k_{006}:k_{005}:k_{004} = 7.9:4.1:1.0 in the measured results, and 2.8:1.7:1.0 in the QCT results, indicating that C−H stretch excitation is more active in promoting reaction than is predicted by the TSH3 surface. Figure 2 shows that these differences in reactivity are due to shifts in the thresholds for reaction, so the comparison with experiment suggests that the TSH3 surface underpredicts the sizes of the threshold shifts with increasing C−H stretch excitation.

In recent studies of the H + H_2O reaction[21] using a new potential energy surface (denoted WSLFH) that was derived from high-quality ab initio calculations, the ratios of stretch excited rate constants were found to be closer to experiment than in the present study. In particular, the ratios k_{004}:k_{003}:k_{002} were found to be 33:8:1 in the QCT results and 16:8:1 in the experiments. Note that the (003):(002) ratio is much larger than the (004):(003) ratio. This result is correlated with the threshold energy, which drops from a large value (around 17 kcal mol^{-1}) for the ground-state reaction to zero with three (or more) quanta of excitation. Three quanta of excitation is somewhat higher than the reaction exoergicity, but Wu and co-workers found that this comparison does not provide a reliable guide to where the threshold energy goes to zero. In particular, they found that less accurate potential surfaces differed significantly from the WSLFH surface with respect to how much excitation is necessary to make the threshold energy go to zero.

The experimental results for HCN(004−006) indicate that the reactivity is behaving in a fashion similar to that of H + H_2O, except that for Cl + HCN, the (005) state marks the break between fast and slow variation with excitation energy. This suggests that the threshold goes to zero for the (005) state, which is about as much above the exoergicity for H + HCN as (003) is for H + H_2O. However, the QCT results do not have a zero threshold energy even for (006) as demonstrated in Figure 2, so we conclude that the TSH3 surface likely does not describe the threshold behavior correctly. This should not be surprising, as the portion of the surface that controls the influence of CH stretch excitation on the threshold energy was not carefully determined on the TSH3 surface.

One other discrepancy between theory and experiment in Table 3 concerns the HCN(302):HCN(402) ratio. This is less than unity in the experimental results, which means that the reactivity increases with increasing C−N stretch excitation. However, it is greater than unity in the QCT calculations, reflecting the threshold behavior in Figure 2. This incorrect result points to an inaccuracy in the TSH3 surface for high C−N stretch excitation, which is a point that we have already noted in discussing Table 1.

As a preliminary conclusion of this section, it has been established by comparing the QCT relative HCN state-specific rate constants and CN rovibrational distributions with the corresponding experimental data that the TSH3 PES used here for the Cl + HCN → HCl + CN reaction can be considered quite accurate for describing the reaction dynamics of a large number of initial HCN states for a broad range of translational energies. With this validation, we turn our attention in the next section to the comparison of the reactivities of the H + HCN → H_2 + CN and Cl + HCN → HCl + CN reactions. Though there have been experimental measurements of the Cl + HCN → HCl + CN stereodynamics,[18,23] the corresponding theoretical work will be considered elsewhere.

IV. Comparison of Cl + HCN with H + HCN

As shown in the previous section, it appears that the primary difference between the Cl and H reactions with vibrationally excited HCN arises from the kinematics associated with

changing the mass of the attacking atom. Although some features of the respective potential surfaces are quite different, those features which are important to the H abstraction under the conditions we have explored are apparently close enough to make this a secondary factor. With this in mind, a useful discussion of the reactivity can be made for the two systems.

Experimentally,[16−18] the internal states of the CN generated in the H (Cl) + HCN → H_2 (HCl) + CN reactions have been used to infer the plausible microscopic mechanisms controlling both reactions. Two main features of the mechanisms have been sought in the experiments. The first deals with whether the CN fragment acts as a spectator or not, while the second considers the relative importance of direct and addition−elimination reaction mechanisms. The latter mechanism is concerned with formation of a H_2CN (HClCN) collision complex. The two points are related, since if during a collision the system remains near the H_2CN (HClCN) minimum for some period of time, the total energy will tend to be distributed between the different degrees of freedom of the complex formed, including the CN fragment. Thus, if energy is transferred to the CN, the CN is prevented from exhibiting merely spectator behavior. Some experimental work on the reverse HCl + CN(v) → Cl + HCN[12,13] and H_2 + CN(v) → H + HCN[24] reactions has shown that rovibrational excitation of the reagent CN has a minor effect on the reaction rate constants. For example, the H_2 + CN(v) → H + HCN experimental rate constants were in general quite successfully reproduced by the reduced dimensional quantum dynamics calculations of Takayanagi and Schatz.[7] Reduced dimensionality quantum dynamics calculations of Bowman et al.[25,26] (based on a simpler potential energy surface) also provide evidence for the CN acting as a spectator-like fragment. However, previous QCT work using the TSH3 PES on the reverse reaction has demonstrated that the CN fragment cannot be considered a pure spectator.[4]

With respect to H (Cl) + HCN, Crim and co-workers[16] estimated from the rovibrational distributions of the CN product that the contribution of the addition−elimination mechanism, which involves complex formation, was more important for Cl + HCN than for H + HCN. In their model, the products of the latter reaction would be formed primarily by direct abstraction while the products of the Cl + HCN reaction would be generated by addition−elimination in addition to the direct abstraction. Conclusions from the experimental work of Gericke and co-workers shifted from exclusion of spectator behavior for CN in a preliminary work[17] to a qualitative spectator model for this fragment, favoring a pure direct abstraction mechanism and neglecting complex formation for both reactions.[18]

Since the QCT approach gives us the coordinates and momenta at any time along the trajectory, we have explored the importance of complex formation in the reactive trajectories for both systems. Figure 3a depicts the percentage of the total cross section due to the PES minimum reaction pathway for Cl + HCN → HCl + CN. It can be seen that at 0.259 eV (Cl + HCN experimental E_T) the contribution is less than 5%. This reaction pathway is only slightly more important for Cl + HCN than for H + HCN, where at 0.83 eV (H + HCN experimental E_T) less than 2% of the reactivity is due to it. The contribution to the reactivity from the addition−elimination mechanism is more important for Cl than for H when HCN is vibrationally excited, but this mechanism is far from being crucial to the total reactivity at moderate translational energies. Thus, the estimates of Crim and co-workers[16] about the importance of the addition−elimination mechanism for the Cl + HCN → HCl + CN reaction would not seem to be born out by the QCT calculations.

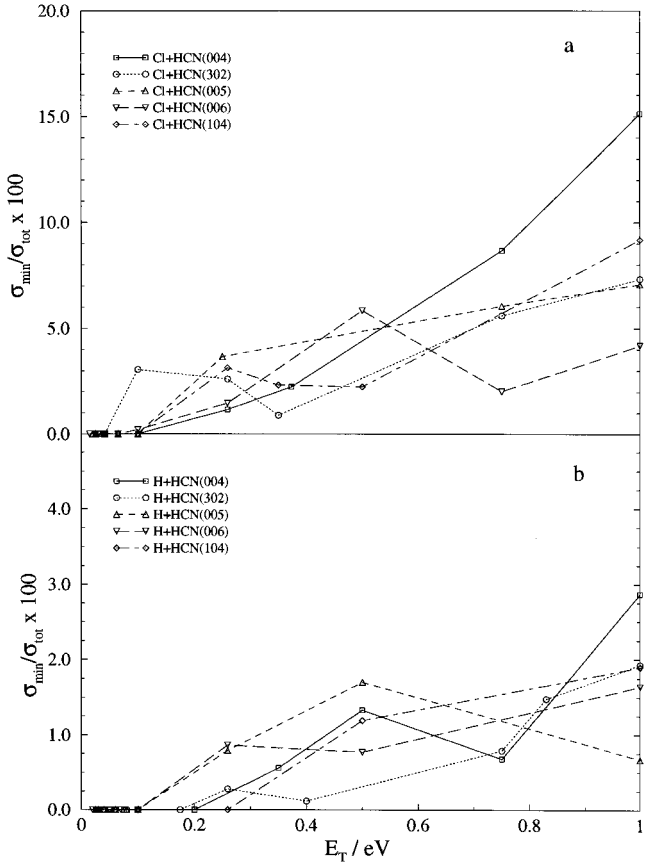

Figure 3. Excitation functions of the Cl (a) and H (b) reactions with vibrationally excited HCN expressed in percentage of the cross sections for the H_2 + CN (HCl + CN) reaction channel due to the reactivity through the H_2CN (HClCN) minimum.

Further, we note that the present model makes the ClHCN well depth much deeper than is found in ab initio calculations,[10] so using a more accurate potential surface should make ClHCN formation even less important.

Concerning the role of the CN fragment as a spectator, the results of our H + HCN work indicated that although there were some correlations between the HCN initial C−N mode and the CN product vibration and also between the HCN rotational state and the CN rotation for the H + HCN → H_2 + CN reaction, the correlations were not as strong as the ones expected from a pure spectator mechanism. In this work, we consider the same initial conditions for both the Cl and H reactions with HCN to verify how different the internal distributions of the CN product are in both reactions. The rovibrational populations of the CN generated with the HCN-(302) and HCN(004) states reacting with Cl and H at 0.259 eV are listed in Table 4. These results show how the CN vibrational populations are more excited for Cl + HCN(004) than for the corresponding reaction with H. In contrast, the same reactions with HCN(302) lead to more excited vibrational populations of CN for the H atom attack. The higher CN vibrational excitation in the Cl + HCN reaction (with no initial C−N stretch excitation) might indicate that the C−N stretching mode is somewhat more coupled to the reaction coordinate in the chlorine reaction than in the hydrogen reaction. The hotter CN vibrational distributions in the reaction with hydrogen when there is initial C−N excitation supports the idea of the stronger correlation between the C−N mode in the reagent HCN and the product CN vibration in the H + HCN → H_2 + CN reaction. Thus, it seems that energy transfer between the different degrees

TABLE 4: CN Rovibrational Distributions from the Reactions of HCN(v_1,0,v_3,j=9) with Cl and H Using the Same Initial Conditions[a]

HCN state	atom	$v'=0$	$v'=1$	$v'=2$	$v'=3$	$\langle E_{VIB}\rangle$	$\langle E_{ROT}\rangle$
004	Cl	0.58 ± 0.05	0.31 ± 0.03	0.09 ± 0.02	0.02 ± 0.01	3.21 ± 0.46	1.21 ± 0.22
004	H	0.75 ± 0.06	0.19 ± 0.03	0.06 ± 0.02		1.81 ± 0.21	0.51 ± 0.11
302	Cl	0.53 ± 0.06	0.32 ± 0.05	0.12 ± 0.03	0.03 ± 0.01	3.80 ± 0.61	1.05 ± 0.25
302	H	0.41 ± 0.03	0.45 ± 0.04	0.11 ± 0.02	0.03 ± 0.01	4.44 ± 0.45	0.46 ± 0.10

[a] E_T = 0.259 eV. Energies in kcal mol^{-1}.

TABLE 5: Average CN Vibrational Energy Resulting from the H + HCN(v_1,0,v_3,j=9) → H_2 + CN(v') Reaction with the Same Total Energy ($E_{TOT} \simeq$ 2.6 eV)[a]

HCN state	HCN E_{INT}/eV	E_T/eV	$\langle E_{VIB}\rangle$/kcal mol^{-1}
002	0.82	1.865	2.22 ± 0.24
004	1.57	0.970	3.79 ± 0.50

[a] The HCN E_{INT} energy does not include the zero-point energy.

of freedom can take place somewhat more easily in the Cl + HCN reaction.

One of the points that could favor the conclusions of Gericke and co-workers about the behavior of the CN fragment as a spectator is the absence of correlation between the initial translational energy and the internal states of the CN product.[16] The QCT results for H + HCN(004) → H_2 + CN at E_T = 0.0388, 0.83, and 1.865 eV indicate that there is only a small dependence of CN vibration on E_T throughout the quite broad E_T range explored. In particular, we find that the CN average vibrational energy ($\langle E_{VIB}\rangle$) increases linearly with E_T, but the CN generated with E_T = 1.865 eV is only 35% more vibrationally excited than the CN arising from thermal conditions (E_T = 300 K, 0.0388 eV (average E_T)) ($\langle E_{VIB}\rangle$ = 3.52 ± 0.26 and 2.61 ± 0.28 kcal mol^{-1} for E_T = 1.865 and 0.0388 eV, respectively). On the other hand, the Cl + HCN(004) → HCl + CN results point to a stronger correlation between CN vibration and collisional energy. In this reaction, the thermal E_T calculations are impractical (because of the long duration of the trajectories), so we have analyzed the CN vibrational distributions in the range of collisional energies from 0.259 to 1.0 eV. Though this E_T interval is 1 eV narrower than the H + HCN interval, the CN vibrational distributions at the larger E_T are 32% more excited than the ones at 0.259 eV ($\langle E_{VIB}\rangle$ = 4.22 ± 0.62 and 3.20 ± 0.30 kcal mol^{-1}, respectively). This would support the idea that the CN mode is more coupled to the reaction coordinate in the Cl + HCN reaction than in the H + HCN reaction.

A deeper analysis of the CN mode couplings reveals that the C−N mode is more coupled to the C−H mode than to E_T. We have carried out QCT calculations using two initial conditions of equal total energy but differently partitioned among initial C−H vibration and initial translational energy for the H + HCN → H_2 + CN reactions. The H + HCN(002) reaction at E_T = 1.865 eV and H + HCN(004) reaction at E_T = 0.97 eV have approximately the same total energy (about 2.6 eV). The latter reaction increases the content of C−H initial vibrational energy with respect to the former and decreases the translational energy to conserve the total energy. The CN vibrational population for the case with more energy in C−H initial vibration and less translational energy is 70% more excited than the one with more translational excitation (see Table 5). That would mean that the C−N mode can couple much more efficiently with the C−H mode than with E_T. The coupling of the C−N and C−H modes would be responsible for making the CN at least a moderately active fragment in the H + HCN reaction.

TABLE 6: Experimental and QCT Thermal (300 K) Relative Rate Constants for H + HCN(v_1,0,v_3,j=9) → H_2 + CN with Different Initial HCN Vibrational States

	exptl[17]	QCT		exptl[17]	QCT
k_{004}/k_{104}		0.9 ± 0.2	k_{005}/k_{004}		1.2 ± 0.2
k_{004}/k_{302}	>4	5.4 ± 0.5	k_{006}/k_{004}		2.2 ± 0.4

TABLE 7: Stationary Point Harmonic Vibrational Frequencies (cm^{-1}) Associated with the X + HCN → HX + CN, X = H, Cl, Reactions[a,b]

X + HCN	H−H−C−N saddle point	Cl−H−C−N saddle point	H_2 + CN	HCl + CN
3449	3139	1754		
2118	2182	2222	2058	2058
750(2)	563(2)	469(2)		
	115(2)	90(2)		
	691i	307i		
			4401	3160

[a] All the data of the HHCN system have been taken from ref 2. [b] The number in parentheses indicates that the frequency corresponds to a doubly degenerate normal vibrational mode.

For completeness, we have also carried out calculations of the relative rate constants for highly excited HCN vibrational states for the H + HCN reaction. Table 6 lists the relative rates. These may be compared with the corresponding rate constants for Cl + HCN by examining Table 3. Again we note that the accuracy of these rate constant estimates is not as good as the indicated statistical uncertainty, due to uncertainties in the treatment of product zero-point energy. The main difference in the relative reactivities occurs for the k_{004}:k_{302} ratio, which is almost 2 times larger for the H reaction than for the Cl reaction. This indicates weaker coupling of the C−N stretch to reaction coordinate motions for H + HCN than Cl + HCN. However, this conclusion is not observed in calculations which consider four quanta of C−H vibrational excitation and zero or one quantum of C−N excitation (HCN(004) and HCN(104)). The rate constant for the Cl + HCN(004) reaction is almost equal to that for Cl + HCN(104). It could be expected from the earlier results that the Cl + HCN(104) rate constant should be higher than the Cl + HCN(004) rate constant, but this is not the case. However, it should be noted that the statistical uncertainties in the rate constant values are relatively large.

One additional comparison of the behavior of the CN fragment in the X + HCN reactions, X = Cl or H, is provided by an analysis of the vibrational frequencies along the intrinsic reaction coordinate (IRC). The fundamental vibrational frequencies of the reactants, products, and saddle point for both reactions have been collected in Table 7. The table shows that the C−N stretch frequency is about the same for the reagents, saddle point, and products for both reactions, but the other high-frequency stretch mode (correlating to the C−H stretch of HCN) is above the C−N stretch frequency for HHCN but below it for ClHCN. To understand what this means, in Figure 4 we plot the three highest frequencies (those which are nonzero for HCN) along the reaction coordinate for both H + HCN (Figure 4a) and Cl

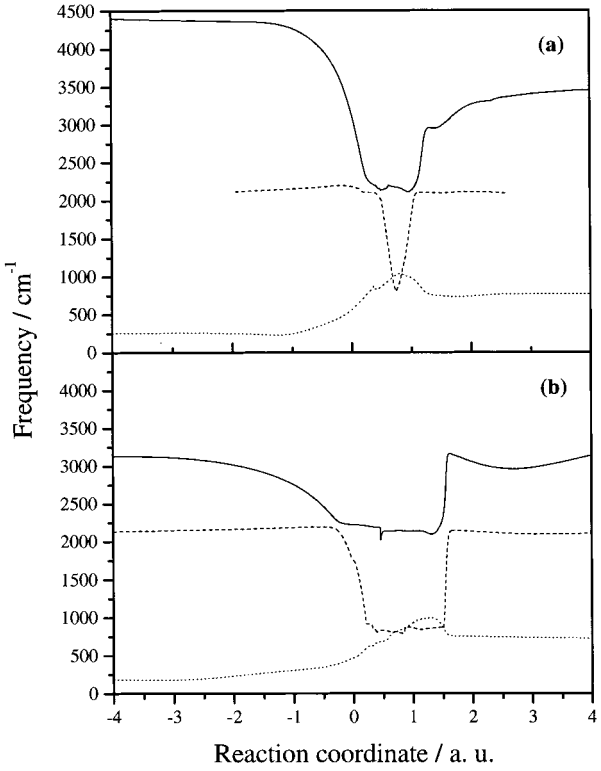

Figure 4. Vibrational frequencies along the minimum energy path for the (a) $H_2 + CN \rightarrow H + HCN$ and (b) $HCl + CN \rightarrow Cl + HCN$ reactions. The solid line is the H_2 or HCl diatom frequency in reagents and the asymmetric HCN stretch in products. The dashed line is the CN frequency in reactants and the symmetric stretch in HCN. The dotted line is the HCN bending frequency. The reaction coordinate values $s < 0$ correspond to the diatom + diatom valley.

+ HCN (Figure 4b). Here we should note that the minimum energy path has been computed considering as reactants (reaction coordinate of the reactants valley <0) the HX + CN asymptote and as products X + HCN, so as to be consistent with a previous calculation.[7] In addition, we note that the frequencies are ill-defined at certain points along the reaction path, so we have "smoothed" the results by omitting a few points.

The figure shows that the C−N mode correlates diabatically with a nearly constant frequency all the way from reactants to products. At the same time, the highest frequency stretch mode (correlating to the C−H stretch of HCN) crosses through the C−N stretch (i.e., shows avoided crossings) in the reagent and product regions. The bend modes are approximately the same for both reactions, which means that the primary difference is in the position of the avoided crossings between the two stretch modes. In particular we note that the crossing occurs farther out in the reactant and product channels for the reaction with Cl than for the reaction with H. This is why the orderings of the modes are different for the saddle point CN and CH stretch modes in Table 7. This crossing occurs farther out in the reactant and product regions for the reaction with Cl because the two stretch frequencies are closer in value for Cl + HCN (where they correspond to H−Cl and C−N, Figure 4b) than for H + HCN (where they refer to H−H and C−N, Figure 4a). If the modes evolve adiabatically during reaction, then the inverted ordering of the two high frequencies at the saddle point makes it possible for C−N stretch excitation to significantly lower the threshold energy for Cl + HCN. However, the splitting between the two stretch frequencies at the point of the avoided crossing is relatively small for both reactions, so it is not clear whether the vibrationally adiabatic behavior that would distinguish the two reactions actually occurs. Indeed, the behavior for Cl + HCN is qualitatively similar to that for $H + H_2O$,[27] where there is a crossing between the vibrationally adiabatic curves associated with the O−H and H−H stretch modes that has no effect on the dynamics because the coupling between the two diabats is too weak. Thus, it is not clear from this analysis whether the behavior of the adiabatic frequencies is sufficient to explain the differences in reaction dynamics between H and Cl + HCN. In the next section we will examine individual trajectories to see whether the adiabatic analysis that we have applied here to the abstraction mechanism is sufficient to explain the reaction dynamics.

It can be concluded from this section that the CN fragment is not a pure spectator in either the Cl or H reaction with HCN, with the Cl reaction showing more significant deviations. In contrast to what might be inferred from the features of the PES, the addition−elimination process is not relevant in the global mechanism, accounting for less than the 5% of the total reactivity for the conditions relevant to the experiments. The insignificant contribution of this reaction pathway helps to validate the model PES used in this work for the Cl + HCN reaction. As the mechanism controlling the Cl + HCN and H + HCN reactions is essentially a direct abstraction, differences between the dynamics of both systems can be regarded as a simple mass effect. The reaction path analysis just presented gives us one way to understand how this mass effect might operate; however, there was uncertainty in the results as to whether this really applies.

V. Microscopic Reaction Mechanisms

To provide deeper insight into the microscopic mechanisms controlling the Cl and H + HCN reaction dynamics, we now analyze the details of the trajectories, including the geometry and potential energy of the system in the strong interaction region. To characterize the strong interaction region, we define the distance RSHELL as the Jacobi coordinate between the attacking atom and the HCN center of mass. Evidently, as the H atom approaches HCN, RSHELL diminishes until it reaches a minimum value ("turning point"). After that, RSHELL becomes gradually larger as the system evolves to products. We have explored the behavior of the potential energy, internuclear distances, and some relevant angles for different RSHELL values corresponding to representative reactant-approaching distances, which are not far from the corresponding values at the saddle point geometry. Three angles will be considered: (a) θ_{X-H-C} (X = H, Cl), defined in terms of the vector between the HCN molecule and the attacking atom and the HC internuclear axis of that molecule; (b) θ_{H-C-N}, the triatom internal angle; (c) the out of plane angle, that is, the angle formed by the vector between the attacking atom to the HCN center of mass and the HCN molecular plane. In this section θ_{X-H-C} will sometimes be called "the angle of attack". For both the Cl and H reactions with HCN, we have investigated two relative translational energy values. One corresponds to the average collision energy of the Cl + HCN system, when the Cl atom is generated from the Cl_2 photodissociation at 355 nm ($E_T = 0.259$ eV). The other one corresponds to the H + HCN relative translational energy, when the H atom is obtained from the CH_3SH photodissociation at 266 nm ($E_T = 0.83$ eV). The HCN(002), -(302), and -(004) initial vibrational states have been considered for both reactions with both translational energies, except for the HCN(002) reaction with $E_T = 0.259$ eV, which is too close to threshold to produce useful results. In the

TABLE 8: Percentage of Reactive Trajectories That Have Reached Different Values of RSHELL for the H + HCN(v_1,0,v_3,j=9) → H_2 + CN Reaction

	RSHELL = 6.5 a_0	RSHELL = 6.0 a_0	RSHELL = 5.5 a_0	RSHELL = 5.0 a_0	RSHELL = 4.5 a_0	RSHELL = 4.0 a_0
E_T = 0.259 eV						
H + HCN(004)	100.0	93.1	56.9	3.7	0	
H + HCN(302)	100.0	88.3	32.0	2.5	0	
E_T = 0.83 eV						
H + HCN(004)	100.0	100.0	84.3	34.6	1.5	0.4
H + HCN(302)	100.0	96.9	78.2	23.6	3.7	0
H + HCN(002)	100.0	100.0	93.5	52.0	0	

TABLE 9: Average Internuclear Distances, Angles, and PES Energies at Different RSHELL Values for the H′ + HCN(004,j=9) → HH′ + CN Reaction at E_T = 0.259 eV

RSHELL/a_0	6.5	6.0	5.5
$\langle r_{H'H}\rangle/a_0$	3.40	2.98	2.01
$\langle r_{H'-C}\rangle/a_0$	5.52	4.99	4.51
$\langle r_{H-C}\rangle/a_0$	2.52	2.26	2.81
$\langle r_{C-N}\rangle/a_0$	2.19	2.21	2.21
$\langle\theta_{H'-H-C}\rangle$/deg	137.7	144.7	138.5
$\langle\theta_{H-C-N}\rangle$/deg	169.1	170.6	168.7
⟨out of plane angle⟩/deg	42.6	45.9	44.6
$\langle E_{PES}\rangle$/kcal mol^{-1}	31.4	25.3	29.9

following sections we first discuss results for H + HCN and then Cl + HCN.

A. H + HCN → H_2 + CN. Table 8 presents the percentage of reactive trajectories as a function of RSHELL. This percentage is 100% for large values of RSHELL, i.e., all reactive trajectories sample large values of RSHELL in the reactant region, and then it decreases to zero for RSHELLs that are sufficiently small. As might be expected, the smallest values of RSHELL for which the percentage is nonzero is smaller for high E_T than for low E_T. In all cases, the turning point of each trajectory occurs for RSHELL values close to the TSH3 H−HCN center of mass saddle point distance (5.6 a_0). The table shows that the range of RSHELL values over which the percentage drops from 100 to 0 is usually 1.0−1.5 a_0, but for H + HCN(002) it is noticeably smaller.

Table 9 presents information about the average values of the internuclear distances, and about the three angles defined above, as a function of RSHELL for the H′ + HCN(004) → H′H + CN reaction with E_T = 0.259 eV. The table shows that the H′H and H′C average distances diminish as RSHELL decreases as a result of the closer approach of the attacking atom to the HCN molecule. The CN average distance remains essentially unaltered by the presence of the attacking atom and is always nearly coincident with the CN equilibrium internuclear distance (2.21 a_0). The HC distance in HCN shows no clear correlation with RSHELL, with an average value that is quite a bit lower than the HC saddle point distance (3.14 a_0). Concerning the angles in the table, the average $\theta_{H'-H-C}$ angle deviates substantially from the collinear (180°) reaction path value. This is not surprising, as the high HCN vibrational excitation allows the system to explore regions of the PES that are well away from the reaction path. No significant variation in this angle with RSHELL is observed for E_T = 0.259 eV. Note that the average HCN angle is much closer to its linear equilibrium value than is the H′−H−C angle, with values that primarily reflect zero-point bending motion. The out of plane angle in Table 9 shows deviations from linearity that are comparable to what is found for the H′−H−C angle. This means that although the coplanar arrangement represents the minimum energy situation, the H′ atom is not forced to collide in the plane formed by the reagent HCN (out of plane angle 0°). The results for the HCN(302) reaction using the same E_T indicate that there are no important differences between the behaviors of the HCN(004) and HCN-(302) reactions. The average internuclear distances have the same trends and values. The angles are also similar, with no significant changes in the attacking angle, $\theta_{H'-H-C}$, except for small RSHELL values (see Table 10). The HCN angle has the same average value (around 171°), showing that triatom bending does not depend on the initial excitation of the HCN molecule.

Examining the average internuclear distances and angles for the H + HCN(004) reaction at a higher translational energy (0.83 eV), differences due to the higher collisional energy soon arise. While it is not surprising that the average internuclear distances are roughly coincident for both energies, the expected broadening in the cone of acceptance with increasing translational energy is relatively small if one compares the average $\theta_{H'-H-C}$ and out of plane angles. The H′−H−C angle is only slightly smaller at higher E_T. Figure 5a−c depicts probability representations for the cosine of the attacking angle, taking into account the RSHELL distance for different HCN vibrational states ((004), (302), and (002)) and E_T = 0.83 eV. For the three HCN modes studied, it can be concluded that larger RSHELL values favor more collinear approach directions. Approaches more perpendicular to the HC internuclear axis of HCN allow for closer approach to the molecular center of mass. In the figure we have not considered the smaller RSHELL values (<5.0 a_0) since their statistics are somewhat poorer.

A more extensive study of the influence of the attacking angle for the H + HCN reaction under different initial conditions is presented in Table 10. The uncertainties in the average angles (around 25%) do not allow us to provide strong insights into the attacking angle behavior. Nevertheless, considering also Figure 5a−c, it appears that there are two different groups of angles associated with different RSHELL values. At larger RSHELL values there are no great differences between the average angles for the two E_T values considered, and also between the different vibrational states with the same E_T. The trajectories with HCN(004) seem to achieve slightly smaller angles than the trajectories with HCN(302), though. However, the trajectories with higher E_T can also reach lower attacking angles. The second group of angles are associated with the lowest RSHELL values, which have been omitted in Figure 5 due to their poor statistics. It can be seen in Table 10 that there are some trajectories that can get much closer to the HCN center of mass, with a small $\theta_{H'-H-C}$ angle for the H′ + HCN(004) reaction with E_T = 0.83 eV. Animation of these very few reactive trajectories (less than 10%) reveals that the H′ atom primarily approaches the N−C end of the HCN molecule until it reaches the small RSHELL value. Afterward, the HCN rotates so that the H′ atom hits H, leading to formation of collinear H′−H−C−N, followed by abstraction. Animation of trajectories reveals that, in steps prior to the onset of the separation to products, the H′−H−C angle is always higher than 150°. More insights into this N−C end approach followed by HCN rotation to favor H abstraction will be commented on in the Cl + HCN analysis.

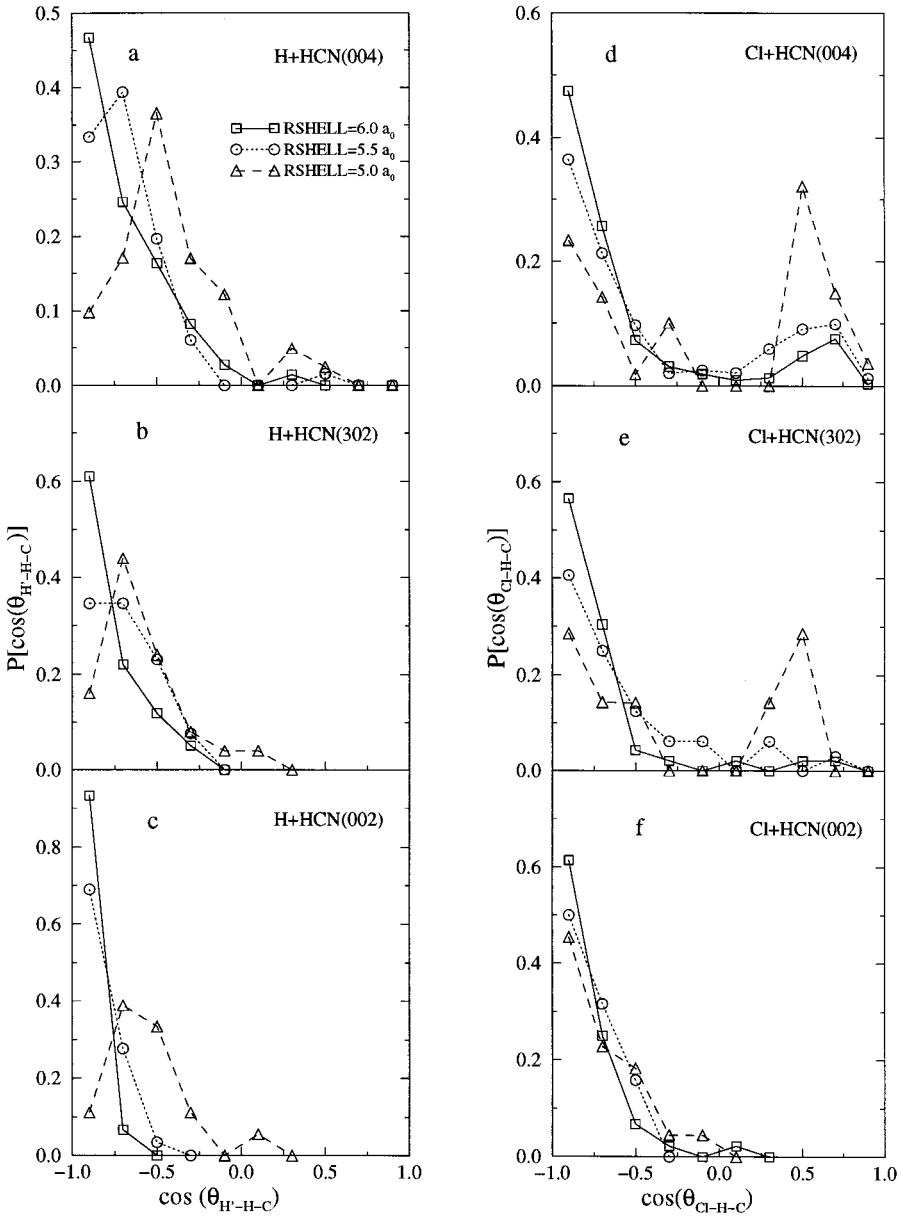

Figure 5. Histogram representation of $\cos(\theta_{X-H-C})$ for the X + HCN → XH + CN, X = H, Cl, reaction with different initial HCN states and E_T = 0.83 eV: (a) H + HCN(004,j=9); (b) H + HCN(302,j=9); (c) H + HCN(002,j=9); (d) Cl + HCN(004,j=9); (e) Cl + HCN(302,j=9); (f) Cl + HCN(002,j=9). The distributions are normalized to unity.

As one final point with the H + HCN analysis, we note that, for the HCN(002) initial state, there is less available energy to surmount the barrier, and this forces the system closer to collinear configurations during reaction.

B. Cl + HCN → HCl + CN. An analogous microscopic reaction mechanism analysis has been performed for the Cl + HCN → HCl + CN reaction. Information about the distribution of RSHELL values analogous to that in Table 8 is presented for the Cl reaction in Table 11. This table shows that the minimum approach distance is larger for the Cl reaction at 0.259 eV while it is smaller at 0.83 eV. The lower energy results, when compared with the corresponding results of the H + HCN reaction, are consistent with the idea that at low energy the Cl moves very slowly and basically "waits" for the vibrating HCN to position the H as close as possible to the Cl, while the corresponding H atom reaction involves more rapid motion so that it penetrates more closely to the HCN before the turning point is reached. At higher translational energy, the Cl atom is able to penetrate to smaller RSHELL values due to the presence of new mechanisms for reaction that will be discussed below.

Details concerning the average internuclear distances and angles for the HCN(004) state at E_T = 0.259 and 0.83 eV point out that the cone of acceptance for the Cl + HCN reaction is broader than for H + HCN. Furthermore, a peculiar behavior is encountered for the lower RSHELL values. In Table 11 it can be seen that there are some trajectories that can reach quite small RSHELL values for 0.83 eV translational energy. Animation of these reactive trajectories reveals that they correspond to the Cl approaching the N−C end of the HCN molecule, much as was briefly noted in the H + HCN collisions. In this case, after the Cl reaches its minimum RSHELL value, the HCN molecule quickly rotates to a nearly linear Cl−HCN geometry, and then abstraction occurs. This is an example of a secondary encounter reaction mechanism, similar to what has been found in certain kinds of heavy−light−heavy triatomic reaction mechanisms. This N−C side attack mechanism is more probable

TABLE 10: Average $\theta_{H'-H-C}$ Angle (deg) at Different Values of RSHELL for the H′ + HCN(v_1,0,v_3,j=9) → HH′ + CN Reaction

	RSHELL = 6.5 a_0	RSHELL = 6.0 a_0	RSHELL = 5.5 a_0	RSHELL = 5.0 a_0	RSHELL = 4.5 a_0	RSHELL = 4.0 a_0
E_T = 0.259 eV						
H + HCN(004)	137.7	144.7	138.5	133.0		
H + HCN(302)	147.0	150.1	137.2	155.9		
E_T = 0.83 eV						
H + HCN(004)	131.3	135.3	138.4	119.3	78.4	37.7
H + HCN(302)	139.6	141.7	132.4	128.1	131.6	
H + HCN(002)	152.1	155.8	148.2	124.6		

TABLE 11: Percentage of Reactive Trajectories That Have Reached Different Values of RSHELL for the Cl + HCN(v_1,0,v_3,j=9) → HCl + CN Reaction

	RSHELL = 6.5 a_0	RSHELL = 6.0 a_0	RSHELL = 5.5 a_0	RSHELL = 5.0 a_0	RSHELL = 4.5 a_0	RSHELL = 4.0 a_0
E_T = 0.259 eV						
Cl + HCN(004)	100.0	90.1	49.3	0		
Cl + HCN(302)	100.0	92.9	33.8	0		
E_T = 0.83 eV						
Cl + HCN(004)	99.0	89.8	59.4	16.3	1.8	0
Cl + HCN(302)	100.0	100.0	68.1	14.9	4.3	0
Cl + HCN(002)	100.0	100.0	82.4	34.4	0	

TABLE 12: Average θ_{Cl-H-C} Angle (deg) at Different Values of RSHELL for the Cl + HCN(v_1,0,v_3,j=9) → HCl + CN Reaction

	RSHELL = 6.5 a_0	RSHELL = 6.0 a_0	RSHELL = 5.5 a_0	RSHELL = 5.0 a_0	RSHELL = 4.5 a_0
E_T = 0.259 eV					
Cl + HCN(004)	116.9	123.7	119.1		
Cl + HCN(302)	123.3	130.0	114.9		
E_T = 0.83 eV					
Cl + HCN(004)	121.3	125.5	113.7	93.2	44.4
Cl + HCN(302)	133.4	137.0	126.1	108.3	82.5
Cl + HCN(002)	137.7	138.1	137.1	130.7	

for the Cl + HCN reaction than for the H + HCN reaction, accounting for 10% of the cross sections at 0.83 eV.

The trajectories corresponding to a N−C attack can be easily distinguished in Table 12 and Figure 5d as they represent the total population at the lower RSHELL values (5.0 a_0 and less). The table presents the average θ_{Cl-H-C} angles for different RSHELL values for all the conditions studied, while the figure depicts the probability distribution associated with the cosine of the attacking angle as a function of RSHELL. It is clearly shown in the figure that the probability of angles corresponding to the N−C end attack drastically increases for the lower RSHELL values. The average attacking angles in Table 12 also decrease dramatically with RSHELL. This arises because trajectories where the Cl approaches the H−C side of HCN (θ_{Cl-H-C} higher than 90°) reach the turning point at higher RSHELL values. This behavior is also observed for the Cl + HCN(302) (see Figure 5e) and H + HCN(004) (Figure 5a) reactions at E_T = 0.83 eV. None of these reactive trajectories have been found for E_T = 0.259 eV or for HCN(002) at E_T = 0.83 eV (Figure 5c,f) in both systems.

Animation of trajectories reveals one more direct mechanism for reaction, in which the Cl atom initially forms a nearly linear Cl−H−C−N structure and then the H atom squeezes out to form rotating HCl while the Cl continues approaching the C atom. The HCl then rotates (the H orbits about the Cl) to briefly make H−Cl−C−N, and then it continues rotating so that there is a hard collision between H and C. Subsequently the HCl departs from CN. This mechanism can be considered to be a secondary collision mechanism in which the Cl first hits HCN, and then rotation of the HCl results in a collision between H and C. Again this is a heavy−light−heavy kinematic effect, which is not seen in the H + HCN reaction. This mechanism accounts for about 10−15% of the total cross section for the Cl + HCN → HCl + CN reaction at E_T = 0.83 eV for HCN-(004), -(302), and -(002). At E_T = 0.259 eV a lower percentage of this mechanism has been found.

Summarizing, we find three distinct abstraction mechanisms for the Cl + HCN reaction. Internuclear distances and the Cl−H−C angle for three trajectories which correspond to these mechanisms are plotted as a function of time in Figure 6. The first type (Figure 6a,d) corresponds to the usual H abstraction process. The second one, plotted in Figure 6b,e, corresponds to the N−C side approach followed by rapid rotation of HCN (Figure 6e) to give a linear ClHCN geometry, followed by abstraction. The third mechanism is shown in Figure 6c,f. Here we see an initial Cl−H−C−N configuration (large Cl−H−C angle) followed by the H−Cl−C−N configuration (small Cl−H−C angle) before the RSHELL value goes through its minimum. Subsequently there is rapid HCl rotation before the two diatomics depart.

The differences found in the microscopic reaction mechanisms of the H + HCN and Cl + HCN reactions lead us to an explanation for the differences in the product vibrational distributions. We have investigated the CN internal distributions arising from the trajectories that undergo the three different mechanisms for the Cl + HCN(004) reaction at E_T = 0.83 eV. At this energy, the global average vibrational energy is $\langle E_{VIB} \rangle$ = 4.00 ± 0.50 kcal mol^{-1}. The cross section for trajectories associated with the mechanism in which the Cl first approaches the N−C side of the HCN molecule is around 8% of the total cross section. The average vibrational energy for these trajectories is 3.65 ± 0.75 kcal mol^{-1}, slightly colder than the global one. However, the third mechanism in which the HCl rotates rapidly while the Cl is attached to the CN produces an average vibrational energy that is twice the global result ($\langle E_{VIB} \rangle$ = 7.94 ± 1.05 kcal mol^{-1}). This mechanism accounts for 10%

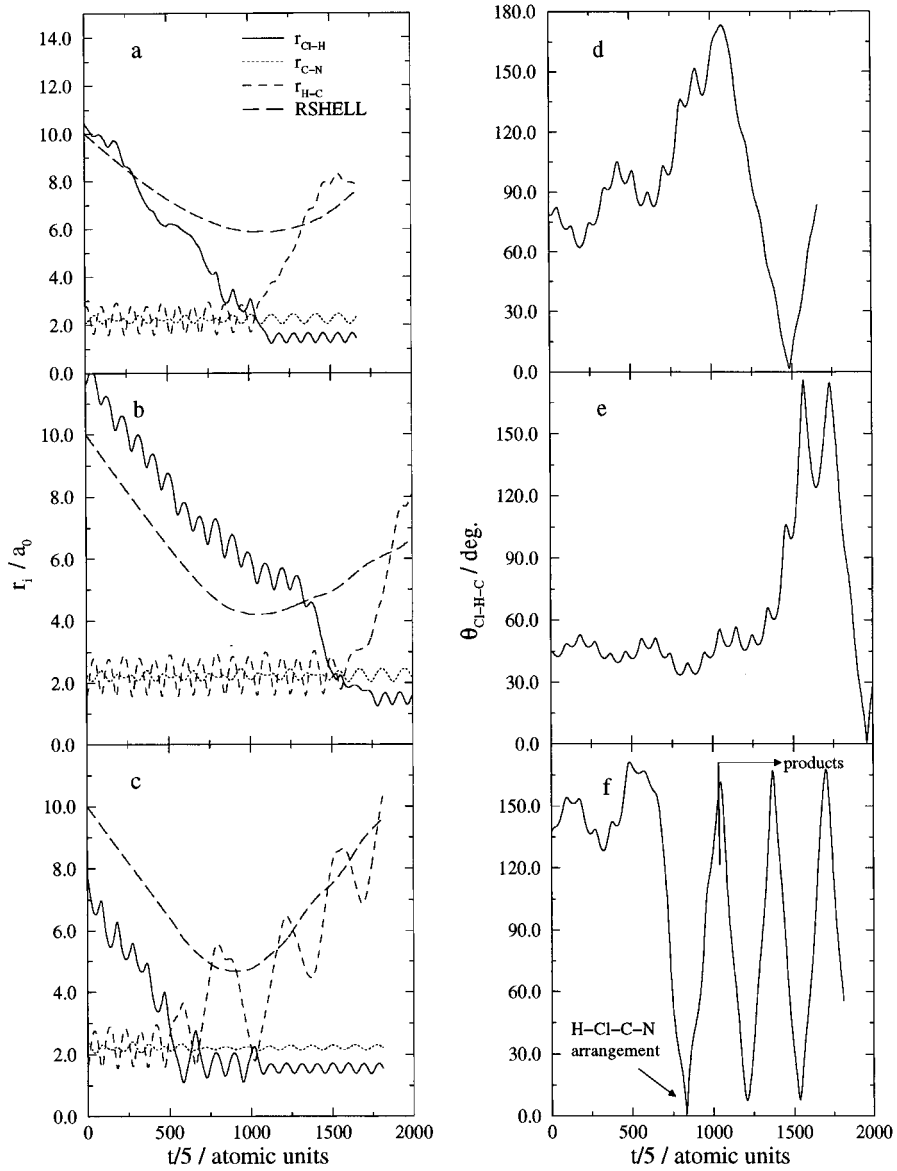

Figure 6. Representative reactive trajectories of the Cl + HCN(004) → HCl + CN reaction at $E_T = 0.83$ eV. Interatomic distances vs time for the (a) direct trajectory, (b) N−C end attack trajectory with HCN quick rotation, and (c) H squeezing out sideways trajectory with H−Cl−C−N configuration formation. In this figure is also presented θ_{Cl-H-C} angle vs time for the (d) direct trajectory, (e) N−C side attack trajectory with HCN quick rotation, and (f) H squeezing out sideways trajectory with H−Cl−C−N configuration formation.

of the cross section, so it increases the overall CN vibrational excitation by 20%. This agrees with the calculated overall change on going from H to Cl at this energy, namely, from 3.09 ± 0.14 to 3.65 ± 0.56 kcal mol^{-1}. We also learn from this analysis that the first mechanism (normal abstraction) does not give vibrational distributions that are much different from those of the sum over mechanisms. This indicates that the vibrationally adiabatic limit, which was mentioned in the previous section, does not apply.

One other important result is that the average rotational energies associated with all three mechanisms are the same, and all are much larger than is found for the H + HCN reaction. Thus, at this energy, the average rotational energy is 0.75 ± 0.12 kcal mol^{-1} for H + HCN and 2.17 ± 0.75 kcal mol^{-1} for Cl + HCN. This indicates that the change in rotational energy from H to Cl is a kinematic effect that applies equally to all three mechanisms. It is not difficult to imagine how this could happen, as the torque applied when Cl and HCN repel each other in the strong interaction region is much larger than that between H and HCN.

VI. Conclusions

In the first part of this work, we presented a QCT study of the Cl + HCN → HCl + CN reaction, using the TSH3 surface which was developed on the basis of ab initio data for the HHCN system. The generally good agreement of not only CN rovibrational distributions, but also relative rate constants for several vibrational states of the reagent HCN, shows the suitability of the TSH3 analytical PES to describe this reaction. This means that the main differences between the Cl and H reactions with HCN to form the corresponding diatomic products can be fairly well explained as due to a mass effect.

A study of the extent to which the spectator model of the CN fragment can be applied to this reaction has shown that although the C−N mode is not as strongly coupled as the C−H mode, it is not completely orthogonal to the modes leading to reaction. In addition, the C−N is more actively involved in the reaction dynamics for the Cl + HCN reaction than for the H + HCN reaction.

The capabilities of the QCT method have been further

exploited by carrying out a detailed analysis of the microscopic reaction mechanism.

A study of the cones of acceptance for the title reactions shows that the Cl atom can abstract the H atom of the HCN molecule with a wider range of Cl−H−C angles than the H attacking atom. A study of the influence of the various types of energy (vibrational and translational) in the direct abstraction process allows us to conclude that the translationally excited attacking atom can reach inner regions (lower minimum approach distances) of the HCN molecule, with a broadened cone of acceptance. A detailed analysis of the reactive trajectories indicates that there are two kinds of "secondary encounter" direct reaction mechanisms in Cl + HCN in addition to the usual direct abstraction. In one of these mechanisms the H atom is "squeezed out sideways" from the ClHCN transition state, and then the HCl rotates rapidly so that the H collides with the CN. In these trajectories, which occur only for the heavy−light−heavy mass combination involving Cl, the CN stretch mode interacts more closely with motions leading to reaction, resulting in CN vibrational distributions that are more highly excited than in H + HCN for initial HCN states having no C−N stretch excitation. The other secondary encounter mechanism involves the Cl striking the N−C side of the HCN first, and then the HCN rotating so that abstraction occurs. This mechanism is also much more important in Cl + HCN than in H + HCN, but the resulting CN vibrational distributions are the same as that for direct abstraction (which is also the same as that for H + HCN). Thus, the greater CN vibrational excitation associated with Cl + HCN is tied to the "HCl rotation" secondary encounter mechanism. Rotational distributions are the same for all of these mechanisms, with considerably more excitation for Cl + HCN than for H + HCN. This indicates that, in all direct abstraction mechanisms, there is greater torque on the HCN when the departing atom is heavier.

We have also shown that the addition−elimination mechanism has only a minor contribution to the global reactivity for both the Cl and H reactions with HCN. It is slightly more important for the Cl reaction, though its contribution to the global reactivity is always less than 5% at translational energies relevant to the experiment.

A more realistic PES for the ClHCN system would be important to describe the contribution to the reactivity due to the ClHCN minimum, as this part of the surface is poorly modeled using the HHCN surface. However, we do not expect ClHCN formation to be more important than we find, as the correct ClHCN minimum is less stable than in the TSH3 PES.

Acknowledgment. This research was supported by NSF Grant CHE-9873892, by the Spanish Ministry of Education and Culture (MEC) through Projects DGES PB98-1209-C02-01 and -02, and by "Generalitat de Catalunya" (Autonomous Government) Project 1998SGR 00008. The "Centre de Supercomputació i Comunicacions de Catalunya (C^4 (CESCA/CEPBA))" is also acknowledged for computation time made available. D.T. thanks the MEC for a Ph.D. studentship and Northwestern University for partial support.

References and Notes

(1) Murrell, J. N.; Carter, S.; Farantos, S. C.; Huxley, P.; Varandas, A. J. C. *Molecular Potential Energy Surfaces*; Wiley: New York, 1984.
(2) ter Horst, M. A.; Schatz, G. C.; Harding, L. B. *J. Chem. Phys.* **1996**, *105*, 558.
(3) Troya, D.; Baños, I.; González, M.; Wu, G.-S.; ter Horst, M. A.; Schatz, G. C. *J. Chem. Phys.* **2000**, *113*, 6253.
(4) Bethardy, G. A.; Wagner, A. F.; Schatz, G. C.; ter Horst, M. A. *J. Chem. Phys.* **1997**, *106*, 6001.
(5) Wang, J.-H.; Liu, K.; Schatz, G. C.; ter Horst, M. A. *J. Chem. Phys.* **1997**, *107*, 7869.
(6) Takayanagi, T.; ter Horst, M. A.; Schatz, G. C. *J. Chem. Phys.* **1996**, *105*, 2309.
(7) Takayanagi, T.; Schatz, G. C. *J. Chem. Phys.* **1997**, *106*, 3227.
(8) Zhu, W.; Zhang, J. Z. H.; Zhang, Y. C.; Zhang, Y. B.; Zhan, L. X.; Zhang, S. L.; Zhang, D. H. *J. Chem. Phys.* **1998**, *108*, 3509.
(9) Manthe, U.; Matzkies, F. *Chem. Phys. Lett.* **1998**, *282*, 442.
(10) Harding, L. B. *J. Phys. Chem.* **1996**, *100*, 10123.
(11) Berkowitz, J.; Ellison, G. B.; Gutman, D. *J. Phys. Chem.* **1994**, *98*, 2744.
(12) Sims, I. R.; Smith, I. W. M. *J. Chem. Soc., Faraday Trans. 2* **1989**, *85*, 915.
(13) Frost, M. J.; Smith, I. W. M.; Spencer-Smith, R. D. *J. Chem. Soc., Faraday Trans.* **1993**, *89*, 2355.
(14) de Juan, J.; Callister, S.; Reisler, H.; Segal, G. A.; Wittig, C. *J. Chem. Phys.* **1988**, *89*, 1977.
(15) Metz, R. B.; Pfeiffer, J. M.; Thoemke, J. D.; Crim, F. F. *Chem. Phys. Lett.* **1994**, *221*, 347.
(16) Pfeiffer, J. M.; Metz, R. B.; Thoemke, J. D.; Woods, E., III; Crim, F. F. *J. Chem. Phys.* **1996**, *104*, 4490.
(17) Kreher, C.; Theinl, R.; Gericke, K.-H. *J. Chem. Phys.* **1996**, *104*, 4481.
(18) Kreher, C.; Rinnenthal, J. L.; Gericke, K.-H. *J. Chem. Phys.* **1998**, *108*, 3154.
(19) Schatz, G. C. *Comput. Phys. Commun.* **1988**, *51*, 135.
(20) Schatz, G. C.; ter Horst, M. A.; Takayanagi, T. In *Computational Methods for Polyatomic Bimolecular Reactions*; Thompson, D. L., Ed.; World Scientific: Singapore, 1998.
(21) Wu, G.-S.; Schatz, G. C.; Lendvay, G.; Fang, D.-C.; Harding, L. B. *J. Chem. Phys.* **2000**, *113*, 3150.
(22) Levine, R. D.; Bernstein, R. B. *Molecular Reaction Dynamics and Chemical Reactivity*; Oxford University Press: Oxford, 1987.
(23) Gericke, K.-H.; Kreher, C.; Reinsch, E. A. *J. Chem. Phys.* **1997**, *107*, 10567.
(24) Sims, I. R.; Smith, I. W. M. *Chem. Phys. Lett.* **1988**, *149*, 565.
(25) Sun, Q.; Bowman, J. M. *J. Chem. Phys.* **1990**, *92*, 5201.
(26) Sun, Q.; Yang, D. L.; Wang, N. S.; Bowman, J. M.; Lin, M. C. *J. Chem. Phys.* **1990**, *93*, 4730.
(27) Schatz, G. C.; Colton, M. C.; Grant, J. L. *J. Chem. Phys.* **1984**, *88*, 2971.